International Microbiology
https://doi.org/10.1007/s10123-023-00393-7

RESEARCH

Genomics analysis of three phosphorus-dissolving bacteria isolated from *Torreya grandis* soil

Qi Wang[1,2] · Chenliang Yu[1,2] · Congcong Kong[1,2] · Hao Zeng[1,2] · Weiwu Yu[1,2,3] · Jiasheng Wu[1,2,3]

Received: 12 April 2023 / Revised: 21 June 2023 / Accepted: 28 June 2023

Abstract

With the increasingly serious problem of phosphorus deficiency in the subtropical zone, chemical fertilizers are widely used. But it pollutes the environment. Phosphorus-solubilizing microorganisms (PSMs) are referred to as a new solution to this problem. We explored the phosphorus-dissolving characteristics of PSB strains isolated from the rhizosphere soil of *Torreya grandis* to provide a theoretical basis for selecting the strain for managing phosphorus deficiency in subtropical soils and also provides a more sufficient theoretical basis for the utilization of PSMs. From 84 strains, three strains exhibiting high phosphorus solubility and strong IAA producing capacity were selected through a series of experiments. The phosphate-solubilizing capacity of the three selected strains W1, W74, and W83 were 339.78 mg/L, 332.57 mg/L, and 358.61 mg/L, respectively. Furthermore, W1 showed the strongest IAA secreting capacity of 8.62 mg/L, followed by W74 (7.58 mg/L), and W83 (7.59 mg/L). Determination by metabolites, it was observed that these three strains dissolved phosphorus by secreting a large amount of lactic acid, aromatic acid, and succinic acid. The genome of these PSBs were sequenced and annotated in this study. Our results revealed that PSB primarily promotes their metabolic pathway, especially carbon metabolism, to secrete plenty organic acids for dissolving insoluble phosphorus.

Keywords Comparative genomics · Phosphorus dissolving · Organic acids · *Torreya grandis*

Introduction

In the process of plant growth and development, phosphorus is the second most necessary nutrient element after nitrogen (Bhattacharyya and Jha 2011). It is involved in multiple physiological and biochemical processes, including photosynthesis, energy generation and transmission, signal transduction, and respiration (Khan et al. 2010; Seema B Sharma et al. 2013; Tian et al. 2021).

Though the soil is naturally rich in phosphorus, most of the amount exists in organic form (Po) which is difficult to get directly absorbed and utilized by plants (Xu et al 2022). Plants absorb P in the form of inorganic phosphate (Pi) from the soil (Wang et al. 2021). However, P easily combines with other substances, such as iron or calcium, to make an insoluble form, resulting in a low concentration of the absorbable P in the soil and affecting the growth and development of plants (Soumare et al. 2019; Penn and Camberato 2019). Especially in tropical and subtropical areas, the leaching of acidic rainwater causes a huge loss of nutrients, thus greatly increasing the amount of fertilizer. In addition, the Fe^{3+} and Al^{3+} rich in the acidic soil quickly fix P through fixation and adsorption reactions (Penn and Camberato 2019).

To counter P deficiency in the soil, the use of chemical fertilizers has been increased widely in agriculture and forestry production (Xing et al. 2021). However, the effective utilization rate of P fertilizer is less than 20% (Alori et al. 2017; Islam 2019; Pradhan et al. 2017). A large amount of phosphate fertilizer is quickly fixed in the soil and gets

Qi Wang and Chenliang Yu contributed equally to this work.

✉ Weiwu Yu
yww888@zafu.edu.cn

✉ Jiasheng Wu
wujs@zafu.edu.cn

1 State Key Laboratory of Subtropical Silviculture, Zhejiang A & F University, Hangzhou, China

2 School of Forestry and Biotechnology, Zhejiang A&F University, Hangzhou, China

3 NFGA Engineering Research Center for Torreya Grandis 'Merrillii', Zhejiang A&F University, Hangzhou 311300, China

Published online: 15 July 2023

converted into a stable form that cannot be used by plants (Mitter et al. 2021). In addition, the extensive use of phosphate fertilizers causes serious damage to the ecological environment (Alori et al. 2017; Manisalidis et al. 2020; Mohamed et al. 2019; Pradhan et al. 2017). Therefore, it is imperative to find a more efficient and environmentally friendly way to manage P deficiency in plants.

P-dissolving bacteria (PSB) isolated from the rhizosphere soil convert ineffective P sources, which cannot be absorbed by plants, into absorbable P sources by secreting various organic acids, including citric acid, formic acid, gluconic acid, malic acid, and oxalic acid (Chungopast et al. 2021; Alori et al. 2017; Liang et al. 2020). In addition to increasing the utilization of available P, PSB also stimulates the growth of plants, especially the growth of lateral roots and root hairs, by secreting various hormones such as auxin (Richardson and Simpson 2011; Wissuwa et al. 2020).

Torreya grandis is a large evergreen economic tree species mainly distributed in southeastern China (Ni et al. 2015). As one of the rare nuts in southeastern China, the seeds of *T. grandis* are not only of good quality but also of unique flavor. It is also rich in several nutrients and biologically active compounds such as alkaloids, flavonoids, and tannins which impart various biological properties, including antioxidant, antifungal, and antiviral activities (Chen et al. 2006, 2014; Dong et al. 2014). Since *T. grandis* is grown in the mountainous region, it needs a large amount of phosphate fertilizer to meet its growth needs.

The focus of this study was to investigate the mechanism of P-solubilization at the genome level by whole-genome sequencing of P-solubilizing microorganisms isolated from the rhizosphere soil of *T. grandis*. While revealing its phosphorus solubilization mechanism, it also provides a potential feasible solution to address the phosphorus deficiency problem in subtropical soils.

Materials and methods

Soil sample

The sample soil was collected from *T. grandis* forest located at the Zhejiang Agriculture and Forestry University. In November 2021, the five-point method was used to collect the healthy *T. grandis* rhizosphere soil. The topsoil was removed, and the sampling depth was kept at 15–25 cm. Then the *T. grandis* root system was taken out, the soil around the root system was removed carefully, and the Rhizosphere soil stuck to the root was collected in a sterile bag using a brush.

Isolation and screening of P-dissolving bacteria

About 5 g of the rhizosphere soil was weighed and taken into a triangular flask containing 45 ml of sterile water. The flask was shaken for 20 min at 220 rpm to make the soil suspension. Following the standard dilution coating plate method, the suspension was successively made into 10^{-2}, 10^{-3}, and 10^{-4} serial dilutions, and each gradient dilution was evenly coated on the inorganic P solid medium (code; HB8549-2, Qingdao Hope Bio-Technology Company). Each concentration was repeated thrice and incubated at 37 ℃ for 7 days. After the optimum bacterial growth, a single colony was selected with a large transparent circle around it and purified five times to obtain a pure culture. Then, the pure culture was grown into the LB medium without antibiotics. The isolated pure 84 strains were inoculated into an inorganic P solid medium and cultured at 37 ℃ for 7 days. Each treatment was conducted in three replicates. The P dissolving capacity was estimated according to the preliminary ratio of the diameter of the P dissolving circle (D) to the diameter of the colony (d), as described by Rodríguez et al. (2006).

Detecting the ability of PSB to dissolve P and secrete auxin

The strains to be tested were inoculated into the LB liquid medium for activation, incubated on a shaking table at 220 $r{\cdot}min^{-1}$ at 37 °C for 1 day, and centrifuged at 8000 $r{\cdot}min^{-1}$ for 5 min. The supernatant was discarded, the pellet was washed thrice with sterile water, and then dissolved to prepare bacterial suspension (to a final bacterial concentration of 1×10^8 $CFU{\cdot}mL^{-1}$). About 5 ml of sterilized inorganic P liquid medium was taken into a 10 ml sterilized centrifuge tube. The bacterial suspension was collected into the 10 ml centrifuge tube according to 2% of the bacterial concentration. Medium without bacteria was used as the control, and three replicates were kept for each treatment. All treatments were incubated on a shaking table at 37 ℃ and 160 $r{\cdot}min^{-1}$ for 5 days. Then, the fermentation broth was centrifuged at 8000 $r{\cdot}min^{-1}$ for 5 min. The content of available P was determined in the supernatant by molybdenum antimony anti-colorimetry (Smith 1999).

The ability of P-dissolving bacteria to secrete IAA was determined by the Salkowski method (Dessaux 1995). The bacterial suspension (bacterial concentration 1×10^8 $CFU{\cdot}mL^{-1}$) of the strains to be tested was added to 5 ml of King B medium according to 2% of the final inoculation amount. The uninoculated medium was used as the control, and each treatment was repeated three times. The culture was incubated on a shaking table at 160 $r{\cdot}min^{-1}$ at 37 ℃ for 7 days. After inoculation, the

culture solution was centrifuged, the supernatant was taken, and mixed with Salkowski colorimetric solution (4.5 g $FeCl_3$, 300 ml ddH_2O, and 587.7 ml of 98% concentrated sulfuric acid, the final volume was made to 1L). Under light-avoiding conditions, the reaction was incubated for 30 min, and the color change was observed. The IAA content was detected by measuring the absorbance at OD_{530} nm.

Molecular identification and phylogenetic analysis

The strains to be tested were inoculated on solid LB media and cultured at 37 °C for 16 h. DNA was extracted using TIANamp Bacteria DNA kit (TIANGEN BIOTECH CO., LTD.). The extracted DNA was used as a template to determine the gene sequence of 16S rDNA for strain identification using the primers (16S17F, AGAGTTTGATCCTGGCTC AG; 1492R, GGTTACCTTGTTACGACTT). The amplified product was purified by the TIAquick Midi Purification kit (TIANGEN BIOTECH CO., LTD.) and sequenced by the Beijing Qingke Biotechnology Co., Ltd.

Organic acid determination assay

The strains to be tested were inoculated into the LB liquid medium for activation, incubated on a shaking table at 220 rpm min^{-1} at 37 °C for 1 day, and centrifuged at 8000 rpm min^{-1} for 5 min. The supernatant was discarded, the pellet was washed thrice with sterile water, and then use non-anti-LB dissolved to prepare bacterial suspension (to a final bacterial concentration of 1×10^8 CFU mL^{-1})., 100 µl of the suspension was added to 5 ml of sterile inorganic P liquid medium, and placed into a 10 ml sterile centrifuge tube. Take no suspension as a control, each treatment was conducted in 3 replicates. All treatments were cultured on a shaker at 37 °C and 160 r·min^{-1} for 5 d. The supernatant was obtained by centrifugation at 8000 rpm for 10 min at 4 °C. An appropriate amount of the supernatant was taken into a 2 mL EP tube, 400 µL of 30% methanol aqueous solution (containing 0.1% formic acid) was added, vortexed for 60 s, and then centrifuged at 12,000 rpm for 10 min at 4 °C. About 10 µL of the supernatant was taken into a 2 mL EP tube, 90 µL of 30% methanol aqueous solution (containing 0.1% formic acid) was added, vortexed for 60 s, and then added to the detection bottle. ACQUITY UPLC® BEH C18 column (2.1 × 100 mm, 1.7 µm, Waters, USA) was used, the injection volume was 5µL, and the column temperature was 40 °C. The mobile phases were A-water (containing 0.1% formic acid) and B-methanol water (with 0.1% formic acid). The gradient elution conditions were 0–3 min, 30% B; 3–5 min, 30–50% B; 5–7 min, 50–90% B; 7–9 min, 90% B;9–13 min, 30% B. Flow rate: 0.4 mL/min (Fiori et al. 2018; Klupczynska et al. 2018; Pawlak et al. 2019).

Scanning electron microscope-based observation

Bacteria cultured in the LB medium for 1 day were collected by centrifuging at 4000 rpm. After obtaining the pellet, it was washed with sterilized ultrapure water. After washing, the bacterial cells were pre-fixed with 1.25% glutaraldehyde fixative at 4 °C for 2 h, then washed with 0.1 mol/L phosphate buffer three times (15 min each), and finally fixed at 4 °C for 2 h with 1% osmic acid. The samples were dehydrated with 50%, 70%, 90%, and 100% ethanol I, II, and III; 100% ethanol + n-amyl acetate (2:1) → 100% ethanol + n-amyl acetate (1:2) → 100% n-amyl acetate I, II, and III (15 min each). After dehydration and replacement, the sample was placed into a sample box and dried in a critical point dryer for about 3 h. Then the conductive adhesive was used to stick the dried sample on the sample table. Finally, the sample was sprayed with gold particles in an ion-sputtering apparatus for 3 min for scanning electron microscope-based observation.

The Instruments and reagents used are as follows: high vacuum coater, Leica Microsystems (Shanghai) Trading Co., Ltd., model (Leica EM AG600), critical point drier, Hitachi, model (HCP-2, field emission scanning electron microscope, Hitachi SU8010). Except for 4% osmic acid, all the reagents were purchased from Tixi 'ai (Shanghai) Chemical Industry Development Co., Ltd. (TCI). Disodium hydrogen phosphate, monosodium phosphate, 25% glutaraldehyde, ethanol, and Isoamyl acetate were purchased from Sinopharm Chemical Reagent Co., Ltd.

DNA extraction and genome sequencing

Genomic DNA of W1, W74, and W83 was extracted using TIANamp Bacteria DNA kit (TIANGEN BIOTECH CO., LTD.). According to the protocol provided by pacbio, G-tube was used to break the DNA sample, repair the damage of the broken DNA sample, repair the end of the DNA, connect the dumbbell connector, digest the exonuclease, and screen the target fragment with bluepippin to obtain the sequencing library.

Genome assembly and annotation

The filtered subreads were assembled using Canu v1.5 software, and then Circlator v1.5.5 was used to cyclize the assembly genome. During genome component prediction, coding genes were predicted using Prodigal v2.6.3. The GenBlastA v1.0.4 program was used to scan the whole genomes after masking predicted functional genes. Putative candidate genes were then identified by searching for non-mature mutations and frame-shift mutations using GeneWise v2.2.0. Transfer RNA (tRNA) genes were predicted with

tRNAscan-SE v2.0, and ribosome RNA (rRNA) genes were predicted with Infernal v1.1.3. Repetitive sequences were predicted using RepeatMasker. PhiSpy v2.3 was used for prophage prediction and CRT v1.2 was used for CRISPR identification. IslandPath-DIMOB v0.2 was used to predict the genomic island in a bacterial genome. antiSMASH v5.0.0 was used to predict secondary metabolic gene clusters, and PromPredict v1 was used for promoter prediction. For functional annotation, the predicted proteins were searched using blast (e-value: 1e-5) against Nr, Swiss-Prot, TrEMBL, KEGG, and eggnog databases. Blast2go was used for GO annotation.

Results

Isolation and screening of P dissolving bacteria in T. grandis rhizosphere soil

A total of 84 bacterial strains were isolated from *T. grandis* rhizosphere soil, of which 24 strains could produce the characteristic P-dissolving transparent circles. After 7 days of the culture, the ratio of the size of the transparent circle produced by the strain to the size of its colony was calculated according to the preliminary screening results of the transparent circle method. The phosphorus dissolving ring ratios of W1, W74, and W83 were the maximum, which were 6.53, 3.26, and 3.67, respectively (Fig. 1A; Table 1). The P dissolving circle of W33 was the smallest, and the D/d value was 1.77. Since the transparent circle method can only be used as a preliminary screening index, other indicators are required for further screening of the strains. In a centrifuge tube containing inorganic phosphorus medium, the strain was cultured for 7 days, and its phosphorus dissolving capacity was determined. The results showed that the P-dissolving capacity of 24 bacterial strains in an inorganic P liquid medium ranged from 259 to 358 $mg{\cdot}L^{-1}$, and differential patterns of the ability to dissolve P were observed among different strains (Table 1). Therefore, combining the above-mentioned results, we selected strains W1, W74, and W83 for further identification and genome sequencing. The indole-3-acetic acid (IAA) content secreted by these strains was also determined. The results revealed that all 24 bacterial strains could produce IAA in King's medium, though differences were observed in the secretion capacity among the strains. In the reaction mix, the color intensity of the

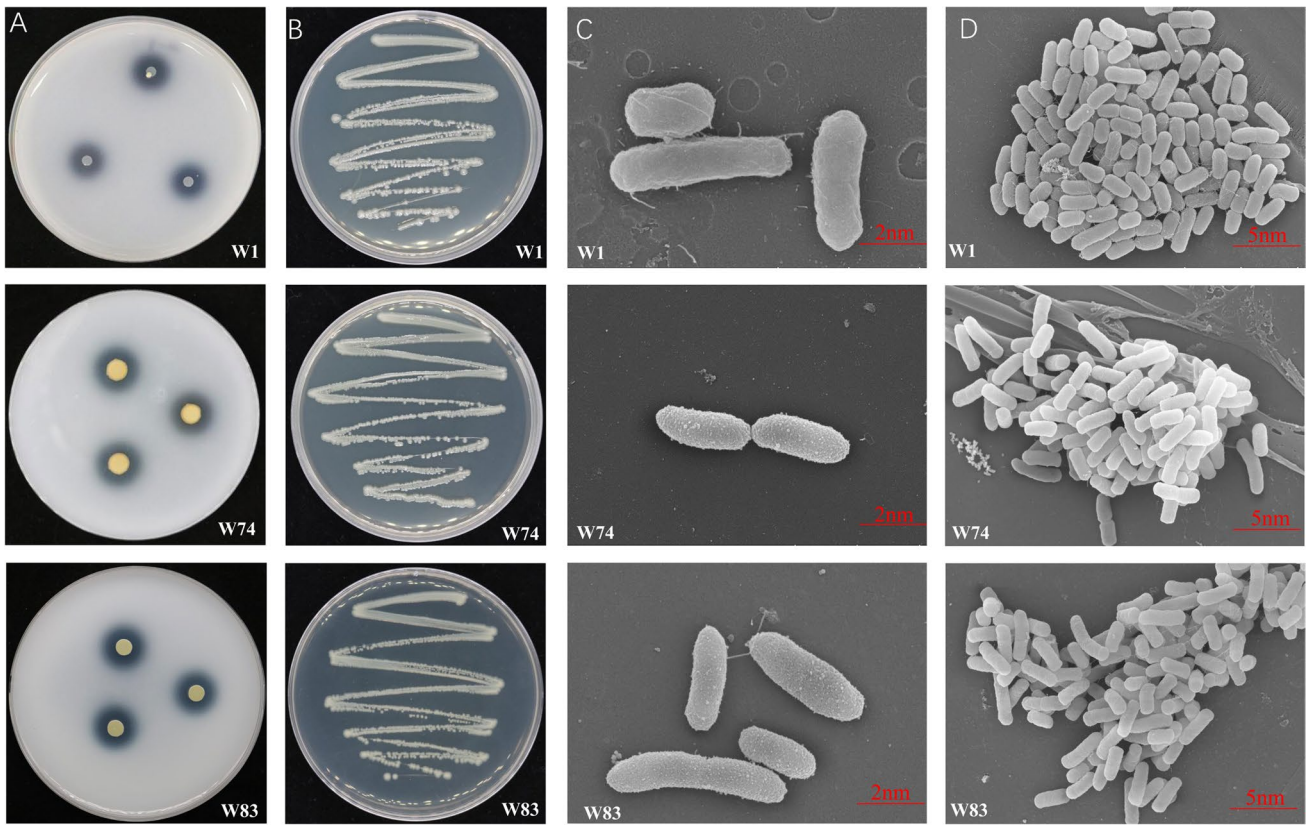

Fig. 1 Cell morphology of three phosphorus-dissolving bacteria. **A** Phosphorus-dissolving ring size of the three strains. **B** The growth morphology of three bacteria cultured for 1 day. **C**, **D** Standard cell morphology of three bacteria with different nano-size under scanning electron microscope

Table 1 Preliminary screening results of inorganic phosphorus solubilizing bacteria

Strain	Transparent circle diameter (D, cm)	Colony diameter (d, cm)	D/d	Available phosphorus ($mg{\cdot}L^{-1}$)	IAA ($mg{\cdot}L^{-1}$)
W1	1.40 ± 0.00	0.22 ± 0.02	6.53 ± 0.80	339.78 ± 9.89	8.62 ± 0.82
W25	1.10 ± 0.10	0.48 ± 0.02	2.27 ± 0.11	259.02 ± 8.03	4.96 ± 0.24
W27	1.33 ± 0.02	0.43 ± 0.02	3.08 ± 0.18	322.58 ± 18.70	5.64 ± 0.94
W28	1.13 ± 0.05	0.45 ± 0.00	2.52 ± 0.25	312.10 ± 18.19	5.08 ± 0.61
W32	1.13 ± 0.11	0.47 ± 0.05	2.43 ± 0.05	308.99 ± 48.89	6.16 ± 0.26
W33	1.13 ± 0.23	0.70 ± 0.17	1.77 ± 0.89	325.69 ± 27.42	5.31 ± 0.80
W38	1.46 ± 0.05	0.50 ± 0.00	2.93 ± 0.11	325.63 ± 23.51	5.30 ± 0.33
W39	1.40 ± 0.00	0.43 ± 0.02	3.20 ± 0.26	334.64 ± 8.31	5.21 ± 0.22
W52	1.30 ± 0.00	0.60 ± 0.1	2.21 ± 0.37	336.95 ± 9.92	5.53 ± 0.13
W58	0.93 ± 0.05	0.50 ± 0.00	1.87 ± 0.11	333.62 ± 6.02	6.63 ± 0.44
W67	1.38 ± 0.02	0.45 ± 0.05	3.10 ± 0.40	318.62 ± 18.59	5.77 ± 0.10
W68	1.23 ± 0.05	0.57 ± 0.05	2.20 ± 0.34	321.09 ± 6.0	4.34 ± 0.10
W71	1.40 ± 0.00	0.47 ± 0.02	3.01 ± 0.17	338.07 ± 22.54	5.48 ± 0.45
W72	1.46 ± 0.05	0.47 ± 0.02	3.15 ± 0.16	350.24 ± 8.79	5.74 ± 0.88
W74	1.23 ± 0.05	0.50 ± 0.00	2.47 ± 0.11	332.57 ± 2.47	7.98 ± 0.36
W75	1.30 ± 0.10	0.45 ± 0.05	2.90 ± 0.10	351.41 ± 21.36	5.19 ± 0.59
W76	1.36 ± 0.11	0.43 ± 0.05	3.20 ± 0.57	338.20 ± 19.28	4.45 ± 0.09
W77	1.36 ± 0.05	0.47 ± 0.02	2.94 ± 0.29	332.18 ± 16.73	4.97 ± 0.48
W78	1.40 ± 0.00	0.43 ± 0.02	3.20 ± 0.15	325.77 ± 22.05	4.37 ± 0.23
W79	1.10 ± 0.17	0.45 ± 0.05	2.44 ± 0.21	311.63 ± 9.72	4.22 ± 0.16
W80	1.30 ± 0.00	0.43 ± 0.05	3.03 ± 0.37	345.68 ± 30.28	4.88 ± 0.25
W81	1.36 ± 0.15	0.45 ± 0.00	3.04 ± 0.33	333.82 ± 14.90	6.74 ± 3.30
W83	1.40 ± 0.00	0.38 ± 0.02	3.67 ± 0.28	358.61 ± 3.01	7.59 ± 0.05
W84	0.90 ± 0.26	0.38 ± 0.02	2.32 ± 0.54	350.26 ± 25.29	7.39 ± 0.26

solution was corresponding to the concentration of IAA. The dark pink color denotes the higher IAA content (Figure S1). The IAA secretion amount of W1, W74, and W83 were 8.62 $mg{\cdot}L^{-1}$, 7.98 $mg{\cdot}L^{-1}$, and 7.59 $mg{\cdot}L^{-1}$, respectively, ranking the top three (Table 1) (Figure S1).

Identification of strains W1, W74, and W83

The strain W1, W74, and W83 were cultured in the solid LB medium for 1 day, and the morphology of the colonies was observed. We observed that the isolated bacteria formed round, regular, moist, convex, gray-white colonies on the LB medium (Fig. 1B). Gram staining, observed under an optical electron microscope, exhibited red color for all three strains, indicating that they are Gram-negative bacteria (Figure S2). As observed under the scanning electron microscope, the morphology of W1 was rod-shaped, while the morphology of W74 and W83 was rod-shaped with irregular wrinkles on the surface and rod-shaped with a rough surface, respectively (Fig. 1C, D). The 16S rDNA sequence of each strain was searched using BLAST against the NCBI database. A phylogenetic tree was constructed by the neighbor-joining method using MEGA11.0 software which revealed that strain W1 had the highest homology with *Pseudomonas,* while W74 showed the highest homology with *Burkholderia*, based on their 16 s rDNA sequence. Furthermore, W83 exhibited the highest homology with *Buttiauxella*. Therefore, W1, W74, and W83 strains were identified as *Pseudomonass*, *Burkholderia*, and *Buttiauxella*, respectively (Figure S3).

Organic acid targeted metabolomics analysis of W1, W74, and W83

After 7 days of culture in centrifuge tubes, the organic acid contents secreted by these strains were determined. It was found that the types and contents of organic acids secreted by the three strains were different from CK (Fig. 2B, C). Lactic acid, succinic acid, malic acid, citric acid, D-glucuronic acid, pantothenic acid, tartaric acid, pyroglutamic acid, and phenyllactic acid were detected in W1, while fumaric acid, maleic acid, malonic acid, and glutaric acid were not identified. Fumaric acid, vanillic acid, adipic acid, hippuric acid, 5-hydroxymethyl-2-furancarboxylic acid, linoleic acid, pyridoxine, 3-indoleacetic acid, and homovanillic acid. Among these, the lactic acid content was highest in W1, reaching 1016.67 $\mu g{\cdot}mL^{-1}$, followed by tartaric acid and succinic acid with concentrations of

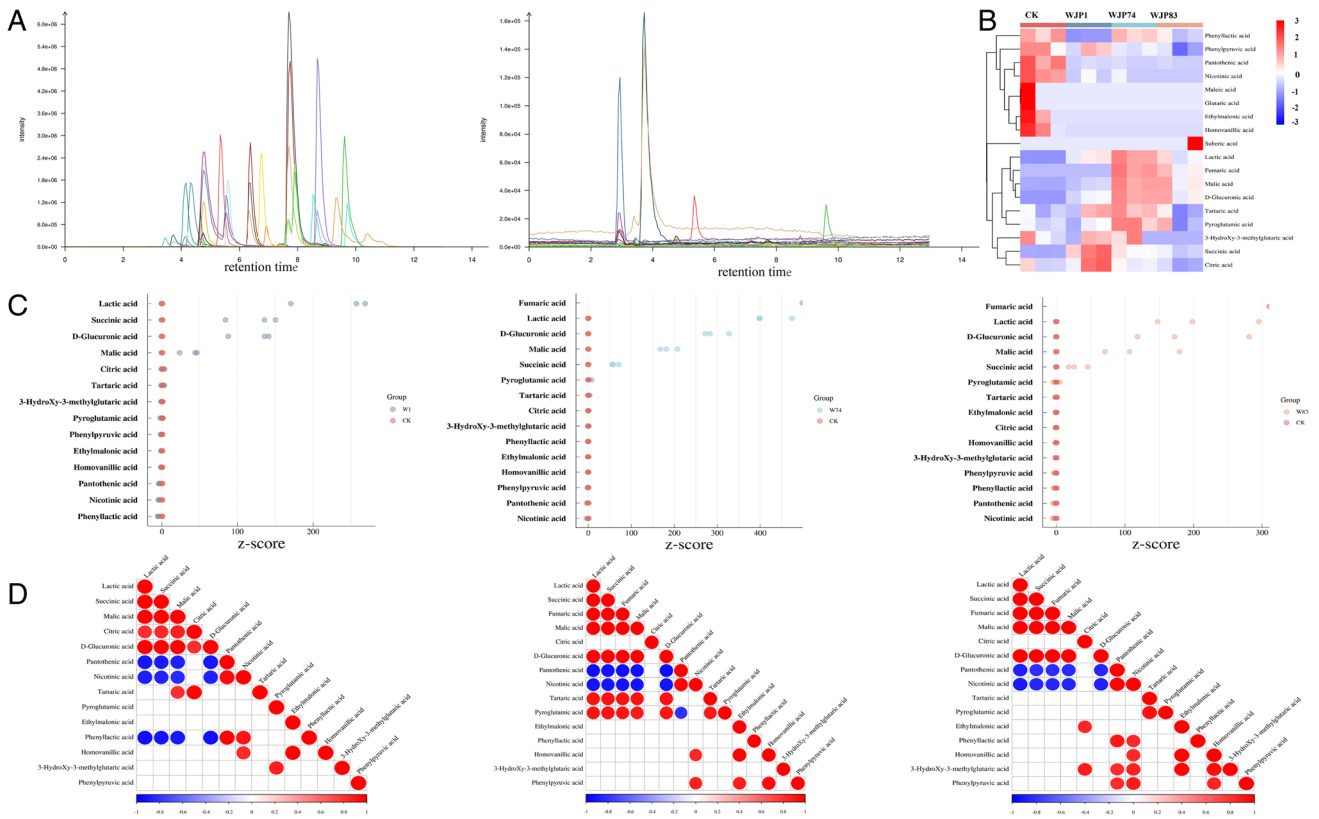

Fig. 2 Organic acid content of three phosphorus-dissolving. **A** Total ion chromatogram. From left to right, the standard total ion chromatogram and sample total ion chromatogram. **B** Hierarchical clustering analysis represented by a heatmap. **C** Z-score is used to measure the content of organic acids at the same level. **D** Correlation heat map between organic acids

445.50 μg·mL^{-1} and 104.83 μg·mL^{-1}, respectively. Next, lactic acid, succinic acid, fumaric acid, malic acid, citric acid, D-glucuronic acid, tartaric acid, pyroglutamic acid, phenyllactic acid, and phenylpyruvic acid were detected in W74, while maleic acid and propionate were not detected. Diacid, glutaric acid, vanillic acid, adipic acid, hippuric acid, 5-hydroxymethyl-2-furoic acid, trimethylglutaric acid, ethylmalonic acid, linoleic acid, pyridoxine, 3-Indoleacetic acid, and homovanillic acid. Among these, the lactic acid content was found to be the highest 1846.67 μg·mL^{-1}, followed by tartaric acid and succinic acid with concentrations of 544.50 μg·mL^{-1} and 53.80 μg·mL^{-1}, respectively. In strain W83, lactic acid, succinic acid, fumaric acid, malic acid, citric acid, D-glucuronic acid, tartaric acid, pyroglutamic acid, phenyllactic acid, and phenylpyruvic acid were detected, while maleic acid and propionate were not detected. Diacid, glutaric acid, vanillic acid, niacin, adipic acid, hippuric acid, 5-hydroxymethyl-2-furoic acid, trimethylglutaric acid, ethylmalonic acid, linoleic acid, pyridine Doxyl, 3-indoleacetic acid, and homovanillic acid. Among these, the lactic acid content was the highest 936.67 μg·mL^{-1}, followed by tartaric acid and succinic acid with concentrations of 247.67 μg·mL^{-1} and 28.00 μg·mL^{-1}, respectively (Fig. 2D, Table S1).

Genomic features of strains W1, W74, and W83

The final assembled genome size of strain W1 was 7.0 Mb, the scaffold N50 was 7.0 Mb, and the GC content was 60.27%. A total of 6214 genes were predicted in the W1 genome, with a full length of 6.17 Mb, accounting for 88.14% of the total genome (Fig. 3A, Tables S2, and S3). Of these, 93 non-coding RNA genes (22 rRNA, 71 tRNA, and no ncRNA) were identified in the W1 genome (Table S4). The final assembled genome size of W74 was 4.01 Mb, the scaffold N50 was 3.98 Mb, and the GC content was 43.76%. A total of 3968 genes were predicted in the W74 genome, with a full length of 3.52 Mb, accounting for 88.66% of the total genome (Fig. 3B, Tables S2, and S3). Of these, 199 non-coding RNA genes (24 rRNA, 83tRNA, and 92 ncRNA) were identified in the W83 genome (Table S4).The final assembled genome size of W83 was 4.82 Mb, the scaffold N50 was 4.71 Mb, and the GC content was 50.12%. A

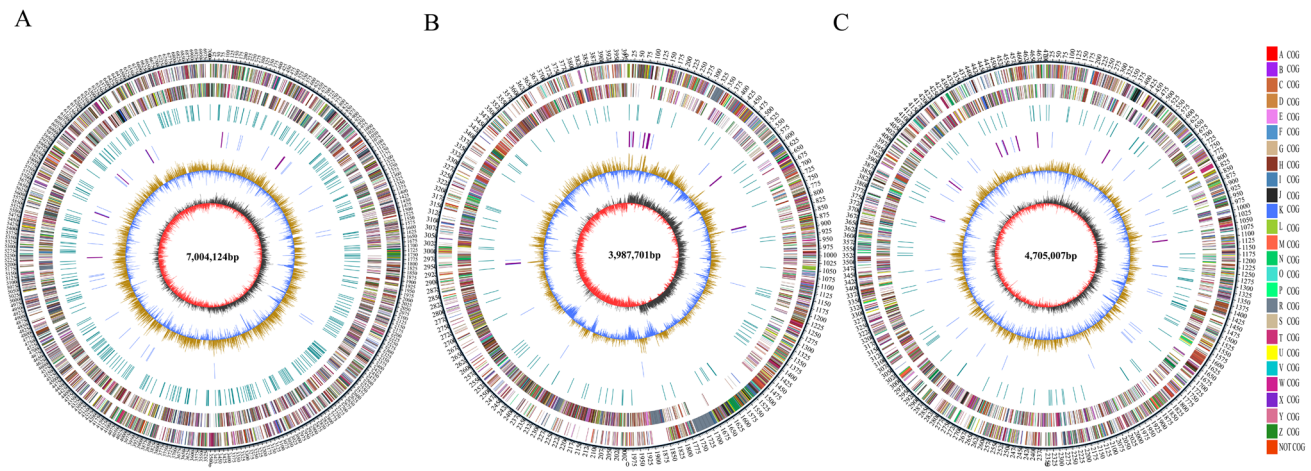

Fig. 3 Circular representation of W1 (**A**), W74 (**B**), and W83 (**C**) genome.The outermost circle is the mark of genome size, each scale is 5 kb; The second and third circles are genes on the positive and negative chains of the genome, and different colors represent different COG functional classifications; the fourth circle is repetitive sequence; the fifth circle is tRNA and rRNA, blue is tRNA, purple is rRNA; the sixth circle is the GC content. The light yellow part indicates that the GC content in this region is higher than the average GC content of the genome. The higher the peak value, the greater the difference between the GC content and the average GC content. The blue part indicates that the GC content in this region is lower than the average GC content of the genome; the innermost circle is GC-skew. Dark gray represents the area where the content of G is greater than C, and red represents the area where the content of C is greater than G

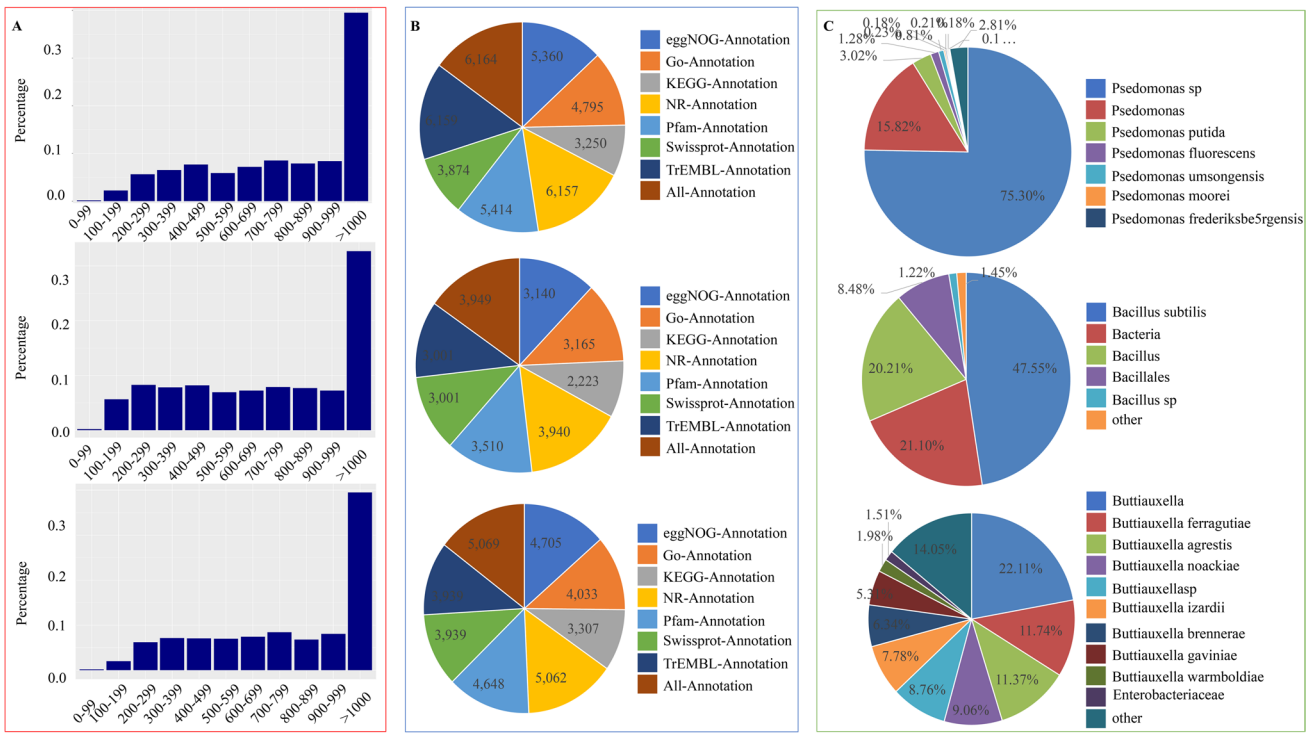

Fig. 4 Protein annotation analysis of three bacteria. **A** Protein length distribution map. The abscissa represents the length of the protein sequence; Proportion represented by ordinate. **B** Protein annotation statistics of seven databases, including eggNOG,GO,kegg, nr, Pfam, Swissprot, and TrEMBL database. **C** The species distribution map of the sequence matched by the Nr database

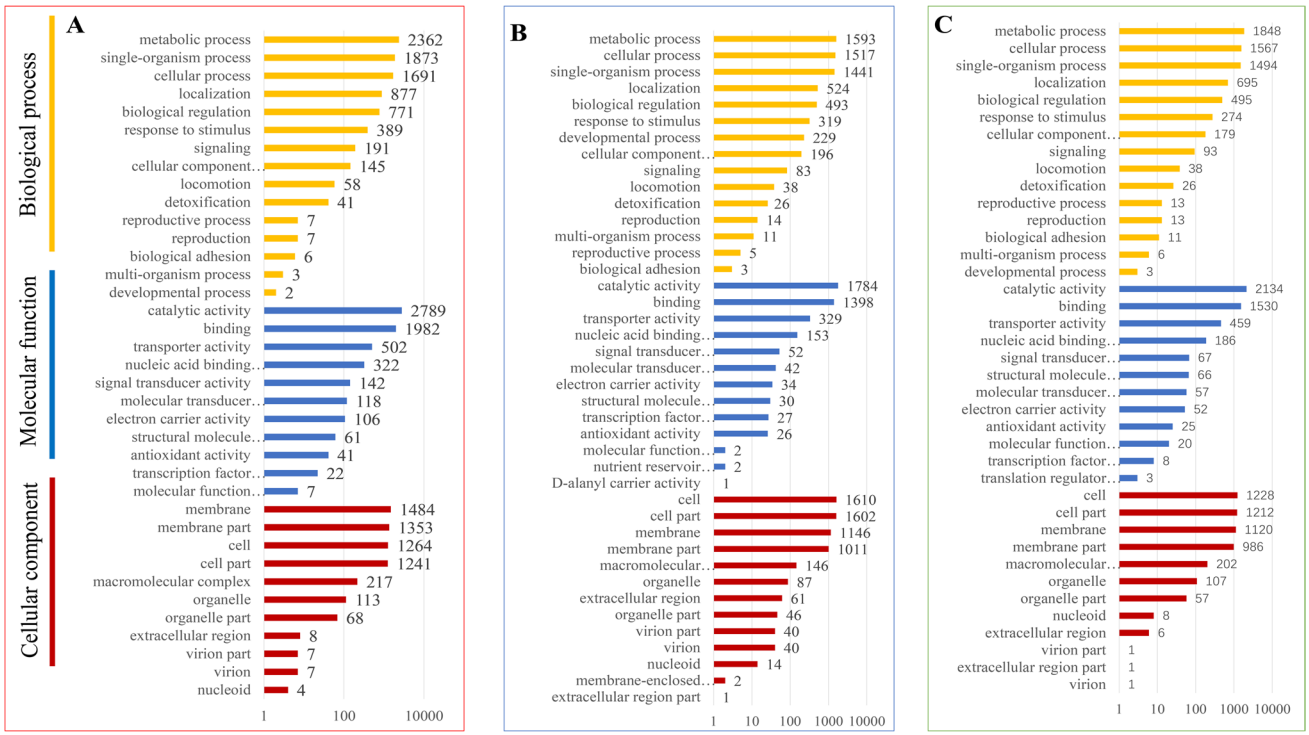

Fig. 5 Go function annotation classification statistics of W1 (**A**), W74 (**B**), and W83 (**C**) proteins based on biological process, molecular function and cellular component.. the left side of the abscissa is the number of genes, the vertical coordinate is the content of GO classification, and the right side is the number of genes

total of 4360 genes were predicted in the W83 genome, with a full length of 4.26 Mb, accounting for 88.66% of the total genome (Fig. 3C, Tables S2, and S3). Of these, 218 non-coding RNA genes (25 rRNA, 83tRNA, and 110 ncRNA) were identified in the W83 genome (Table S4).

Functional annotation and KEGG pathway analysis of genes identified in strains W1, W74, and W83

We made statistics on the protein length distribution of the three strains and the annotations in different databases, and found that the sequence distribution of the three strains and the annotations between different databases were different (Fig. 4A, B). After BLAST alignment of the gene and protein sequences obtained from three strains against the NR database which revealed that the protein sequences of W1 were mainly aligned to 10 species, and the top three species with the highest homology were *Pseudomonas sp.* (75.30%), *Pseudomonas* (15.82%), and *Pseudomonas putida* (3.02%). The protein sequence comparison of W74 showed that five species occupied nearly 99% of the total, and the top three species with the highest homology were *Bacillus subtilis* (47.55%), *Bacteria* (21.10%), and *Bacillus* (20.21%). The protein sequences of W83 exhibited the highest homology with 10 species, of which the top three were *Buttiauxella* (22.11%), *Buttiauxella ferragutiae* (11.74%), and *Buttiauxella agrestis* (11.37%) (Fig. 4C).

To better understand the species-specific functional classification of genes identified from these three strains, we conducted gene ontology (GO) and the Kyoto Encyclopedia of Genes and Genomes (KEGG) classification analyses. In strain W1, GO terms were assigned to a total of 20,281 single genes belonging to 37 subcategories. Biological processes accounted for the main proportion in GO annotation (8423 genes, 41.53%), followed by molecular functions (6092 genes, 30.04%) and cellular components (5766 genes, 28.43%). The biological processes metabolic processes (28.04%), single-organism processes (22.24%), and cellular processes (20.08%) were highly enriched. The top three molecular functions were catalytic activity (45.78%), binding (32.53%), and transporter activity (8.24%), while the top three cellular components were membrane (25.74%), membrane parts (23.47%), and cell (21.92%) (Fig. 5A). In strain W74, GO terms were assigned to a total of 16,115 single genes belonging to 41 subcategories. Biological processes accounted for a major proportion of GO annotation (6429 genes, 39.89%), followed by cellular components (5806 genes, 36.03%), and molecular functions (3880 genes, 24.08%). The highly enriched biological processes were metabolic processes (24.78%), cellular processes (23.60%), and single-organism processes (22.41%). The top three cellular components were cells (27.73%), cell parts (27.59%),

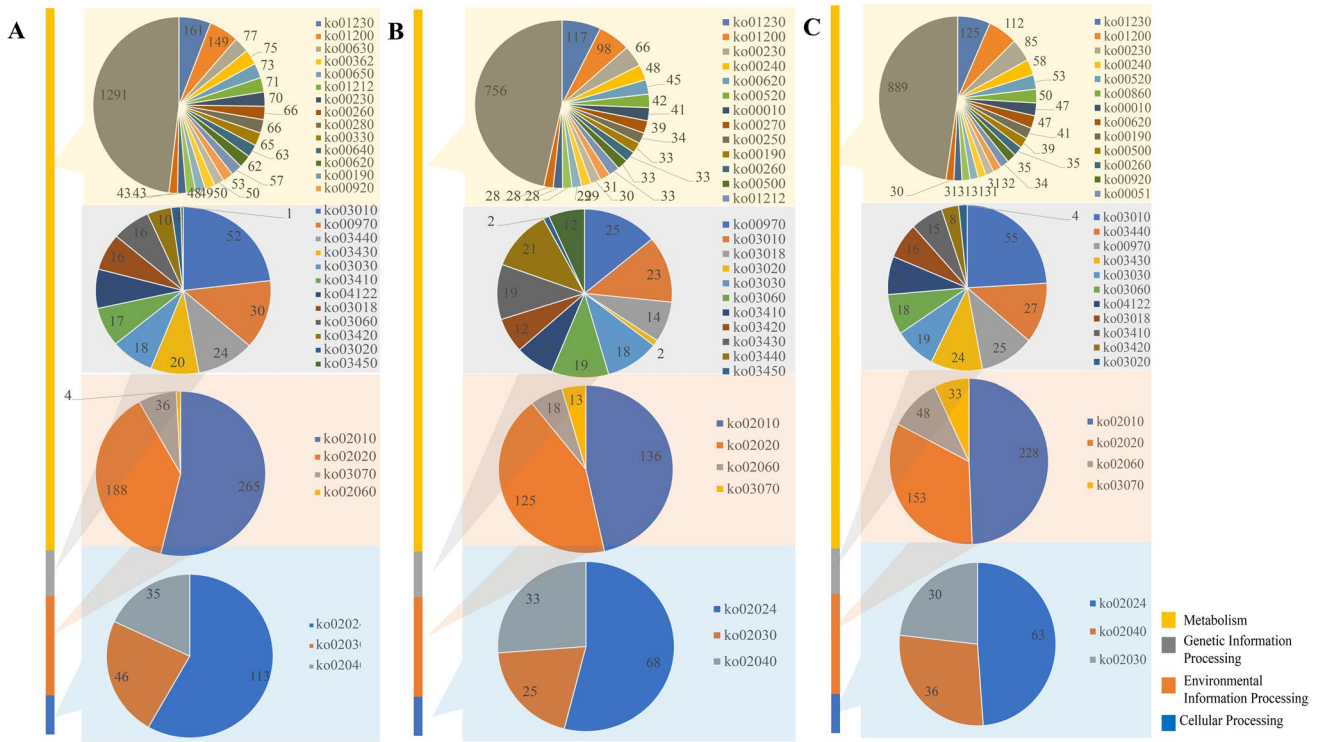

Fig. 6 KEGG function annotation classification statistics of W1 (**A**), W74 (**B**), and W83 (**C**) proteins. The proteins were assigned to different KEGG terms. Different color blocks represent different terms, from top to down, "metabolism," "genetic information processing," "environmental information processing," and "cellular processes." Proportion of proteins in each second level term in "metabolism," "genetic information processing," "environmental information processing," and "cellular processes" were shown

and membrane (19.74%), while the top three molecular functions were catalytic activity (45.98%), binding (36.03%), and transporter activity (8.48%) (Fig. 5B). In strain W83, a total of 16,291 single genes were assigned to GO terms belonging to 39 subcategories. Biological processes accounted for the major proportion of GO annotation (6755 genes, 41.46%), followed by cellular components (4929 genes, 30.26%), and molecular functions (4607 genes, 28.28%). The top three biological processes were metabolic processes (27.36%), cellular processes (23.20%), and single-organism processes (22.12%). The top three cellular components were cells (24.91%), cell parts (24.59%), and membrane (22.72%), while the top three molecular functions were catalytic activity (46.32%), binding (33.21%), and transporter (9.96%) (Fig. 5C).

Organisms require the coordinated expression of multiple genes to perform specific functions; therefore, to further explore the P-dissolving pathway of P-dissolving bacteria, we also classified and counted the KEGG function annotation of the protein. The KEGG annotation of the proteins of the three strains found that the differences mainly focused on metabolism, rather than genetic information processing, environmental information processing and cell process. In strain W1, 3250 genes were annotated into 119 pathways, some of which were found to be involved in multiple metabolic pathways. In metabolic pathway, 20 annotated pathways accounted for 51.86% of the total KEGG annotation. Of these, the top ten pathways were biosynthesis of amino acids (6%), carbon metabolism (5.55%), glyoxylate and dicarboxylate metabolism (2.87%), benzoate degradation (2.79%), butanoate metabolism (2.72%), fatty acid metabolism (2.65%), purine metabolism (2.61%), valine, leucine and isoleucine metabolism (2.46%), glycine, serine and threonine metabolism (2.46%), and arginine and proline metabolism (2.42%) (Fig. 6A). In strain W74, 2223 genes were annotated into 112 pathways, some of which were found to play a role in multiple metabolic pathways. In metabolic pathway, the 20 annotated pathways accounted for 52.51% of the total KEGG annotation. Of these, the top ten enriched pathways were biosynthesis of amino acids (7.35%), carbon metabolism (6.16%), purine metabolism (4.15%), pyrimidine metabolism (3.01%), pyruvate metabolism (2.83%), amino sugar and nucleotide sugar metabolism (2.64%), glycolysis or gluconeogenesis (2.58%), cysteine and methionine metabolism (2.45%), alanine, aspartate and glutamate metabolism (2.14%), and glycine, serine and threonine metabolism (2.07%) (Fig. 6B). In strain W83, 2972

Table 2 ANI analyses between W1 and other representative

Reference genomes	Query genome of WJP1	
	ANIb and [aligned nucleotides] (%)	ANIm [aligned nucleotides] (%)
Pseudomonas vancouverensis strain BS3656 genome assembly, chromosome	84.48 [74.88]	88.59 [51.83]
Pseudomonas izuensis DNA, complete genome	86.84 [77.97]	89.68 [63.65]
Pseudomonas sp. PP3 genome assembly, chromosome	86.46 [74.37]	89.54 [58.86]
Pseudomonas reinekei strain BS3776 genome assembly, chromosome	86.26 [73.02]	89.41 [57.14]
Pseudomonas fluorescens strain LBUM677 chromosome, complete genome	83.45 [68.66]	88.02 [44.99]
Pseudomonas koreensis strain CRS05-R5 chromosome, complete genome	83.55 [68.90]	88.06 [45.90]
Pseudomonas koreensis strain D26 chromosome, complete genome	82.58 [67.47]	87.69 [41.14]
Pseudomonas siliginis strain OTU6BANIB1 chromosome, complete genome	82.61 [67.30]	87.67 [41.29]
Pseudomonas atacamensis strain SWRI76 chromosome, complete genome	82.68 [67.58]	87.67 [41.54]
Pseudomonas atacamensis strain SM1 chromosome, complete genome	82.72 [67.36]	87.67 [41.35]
Pseudomonas sp. S150 chromosome, complete genome	83.41 [68.64]	88.02 [44.90]
Pseudomonas moraviensis strain BS3668 genome assembly, chromosome 1	82.66 [66.67]	87.62 [41.37]
Pseudomonas siliginis strain OTU6MEDAA1 chromosome, complete genome	82.70 [67.52]	87.63 [41.87]
Pseudomonas siliginis strain OTU6MONEA1 chromosome, complete genome	82.67 [67.02]	87.68 [41.36]
Pseudomonas siliginis strain OTU6ESPEB1 chromosome, complete genome	82.72 [67.38]	87.65 [41.69]
seudomonas siliginis strain OTU6BAGNBB1 chromosome, complete genome	82.64 [67.85]	87.63 [41.72]
Pseudomonas siliginis strain OTU6MONTID1 chromosome, complete genome	82.63 [67.20]	87.69 [41.32]
Pseudomonas moraviensis strain OTU5BARRA1 chromosome, complete genome	82.70 [66.58]	87.65 [41.22]
Pseudomonas moraviensis strain OTU5MASSA1 chromosome, complete genome	82.70 [66.59]	87.64 [41.09]
Pseudomonas moraviensis strain OTU5VILLAA1 chromosome, complete genome	82.70 [66.64]	87.63 [41.37]
Pseudomonas putida strain PgBE89 chromosome	83.46 [68.72]	88.00 [45.14]
Pseudomonas sp. AO-1 chromosome, complete genome	83.27 [69.00]	87.95 [44.62]
Pseudomonas iranensis strain SWRI54 chromosome, complete genome	82.66 [67.54]	87.65 [41.54]
Pseudomonas monsensis strain PGSB 8459 chromosome, complete genome	83.28 [68.99]	87.97 [44.28]
Pseudomonas fluorescens strain G7 chromosome, complete genome	83.51 [71.14]	88.06 [46.77]
Pseudomonas umsongensis strain CY-1 chromosome, complete genome	91.88 [82.61]	93.60 [77.15]
Pseudomonas sp. 3–2 chromosome, complete genome	83.68 [70.53]	88.17 [47.83]
Pseudomonas umsongensis strain BS3657 genome assembly, chromosome 1	91.90 [83.22]	93.54 [77.92]
seudomonas koreensis strain BS3658 genome assembly, chromosome 1	83.55 [68.95]	88.02 [46.25]

genes were annotated into 116 pathways, some of which were observed to play a role in multiple metabolic pathways. The 20 annotated pathways accounted for 52.13%of the total KEGG annotation, and the top ten enriched pathways were biosynthesis of amino acids (7.20%), carbon metabolism (5.97%), purine metabolism (4.53%), pyrimidine metabolism (3.09%), amino sugar and nucleotide sugar metabolism (2.83%), porphyrin and chlorophyll metabolism (2.67%), glycolysis or gluconeogenesis (2.51%), pyruvate metabolism (2.51%), oxidative phosphorylation (2.18%), and starch and sucrose metabolism (2.08%) (Fig. 6C). Go and KEGG annotations of the genes deduced in three strains provided comprehensive information on specific biological processes and pathways of PSBs.

Comparative genomic analysis

Compared with the published genomes, the W1 genome and the *P. umsongensis* strain BS3657 genome had the highest average nucleotide identity (ANIb) of 91.90%, indicating that the two belong to the same species (Table 2). The sequenced W74 genome and the *B. ambifaria* strain MC40-6 genome had the highest ANIb of 69.41%, indicating that these two sequences belong to the same species (Table 3). And the sequences of the W83 strain and the Buttiauxella sp. strain 3AFRM03 showed the highest ANIb of 86.40%, indicating that these two belong to the same species (Table 4).

Collinearity analysis is one of the important means to study species evolution. Using the ANIb analysis value

Table 3 ANI analyses between W74 and other representative

Reference genomes	Query genome of WJP74	
	ANIb and [aligned nucleotides] (%)	ANIm [aligned nucleotides] (%)
Burkholderia_sp._NRF60-BP8_chromosome 1	66.03 [2.62]	90.74 [0.56]
Burkholderia_sp._MSMB0856_chromosome 1	65.83 [2.68]	87.80 [0.57]
Burkholderia_sp._MSMB0856_chromosome 2	69.19 [1.62]	88.60 [0.56]
Burkholderia_sp._MS455_chromosome 3	65.97 [2.65]	89.05 [0.57]
Burkholderia_ sp_ MS389 chromosome 1	65.92 [2.60]	88.84 [0.57]
Burkholderia_sp._LAS2_chromosome 1	65.36 [2.97]	87.69 [0.57]
Burkholderia_sp._KBS0801_chromosome 2	69.23 [2.62]	88.85 [0.56]
Burkholderia_sp._JP2-270_chromosome 2	68.87 [1.68]	88.35 [0.56]
Burkholderia_sp._KBS0801_chromosome 1	65.72 [2.73]	88.10 [0.57]
Burkholderia_sp._JP2-270_chromosome 1	65.71 [2.73]	87.97 [0.57]
Burkholderia_ pyrrocinia_ strain_ Hargis_ chromosome 1	65.81 [2.54]	87.90 [0.57]
Burkholderia_cepacia_strain_FDAARGOS_388_chromosome 1	66.17 [2.55]	90.52 [0.57]
Burkholderia_cepacia_strain_FDAARGOS_345_chromosome 1	66.19 [2.55]	87.82 [0.57]
Burkholderia_cepacia_ATCC_25416_strain_UCB_717_chromosome 1	66.19 [2.55]	89.16 [0.57]
Burkholderia_cenocepacia_strain_VC7848_chromosome	5.20 [3.42]	8.11 [0.57]
Burkholderia_cenocepacia_strain_toggle3_chromosome 1	66.04 [2.61]	87.81 [0.57]
Burkholderia_cenocepacia_strain_R-12632_genome_assembly	65.94 [2.61]	89.08 [0.57]
Burkholderia_cenocepacia_strain_FL-5–3-30-S1-D7_chromosome 1	65.98 [2.65]	87.90 [0.57]
Burkholderia_cenocepacia_strain_CR318_chromosome 1	65.87 [2.66]	90.45 [0.57]
Burkholderia_cenocepacia_MC0-3_chromosome 1	65.83 [2.70]	87.89 [0.57]
Burkholderia_cenocepacia_HI2424_chromosome_1	65.82 [2.70]	90.56 [0.57]
Burkholderia_ambifaria_strain_FDAARGOS_1027	65.83 [2.59]	90.46 [0.57]
Burkholderia_ambifaria_strain_BJQ0010_chromosome 1	65.94 [2.57]	89.83 [0.57]
Burkholderia_ambifaria_strain_B21-008_chromosome 1	65.93 [2.58]	89.83 [0.57]
Burkholderia_ambifaria_strain_B21-006_chromosome 1	65.65 [2.62]	88.06 [0.57]
Burkholderia_ambifaria_strain_B21-004_chromosome 1	65.84 [2.69]	88.06 [0.57]
Burkholderia_ambifaria_MC40-6_chromosome 2	69.41 [1.49]	88.39 [0.56]
Burkholderia_ambifaria_MC40-6_chromosome 1	65.75 [2.63]	90.55 [0.57]
Burkholderia_ambifaria_AMMD_chromosome 1	65.82 [2.59]	88.64 [0.57]

obtained using the genome data as a reference, we selected the top two strains for collinearity analysis which revealed that W1, *Pseudomonas umsonensis* (BS3657), and *P. umsonensis* (CY-1) exhibit very high collinearity. Various sequences showed a high degree of linear intercorrelation among three species, and the collinearity was mainly concentrated in one chromosomal segment (Fig. 7A). W74 exhibited high collinearity with *Burkholderia ambifaria* (MC40-6) and *B. sp.* (MSMB0856). Unlike WJP1, its sequence fragments were mainly concentrated in three chromosomal fragments (Fig. 7B). Furthermore, W83, *Buttiauxella agristis* (DSM9389), and *B.sp.* (3AFRM03) showed very high collinearity, and a large number of sequence fragments concentrated on a single chromosomal segment (Fig. 7C).

Discussion

Due to the decreasing phosphate rock resources, the high cost of chemical phosphate fertilizers, and large ecological environment pollution (Mohamed et al. 2019), it is of utmost importance to optimize the use of P-dissolving microorganisms in agriculture and forestry. However, our understanding of P-dissolving bacteria is very limited to date. Therefore, we have sequenced and analyzed the whole genome of three phosphorus-dissolving bacteria isolated from the soil of T grandis, a subtropical tree, in order to effectively reveal its phosphorus-dissolving mechanism, expand the theoretical basis for further large-scale and efficient use of these strains, and also provide a new solution to solve the problem of phosphorus deficiency in subtropical soil.

Table 4 ANI analyses between W83 and other representative

Reference genomes	Query genome of WJP83	
	ANIb and [aligned nucleotides] (%)	ANIm and [aligned nucleotides] (%)
Buttiauxella_agrestis_DSM9389	84.08 [76.53]	86.40 [66.62]
Buttiauxella_sp._3AFRM03	86.40 [79.73]	87.81 [77.63]
Cedecea_neteri_strain_ND14a	77.43 [61.74]	83.96 [24.21]
Enterobacter_asburiae_MRY18-106	75.30 [59.75]	84.18 [15.40]
Enterobacter_sp._JUb54_strain_RIT712	74.86 [57.55]	84.41 [13.16]
Enterobacter_sp._RHB15-C17_chromosome	75.43 [61.22]	84.22 [15.59]
Klebsiella_aerogenes_strain_18-2341_chromosome	74.62 [58.14]	84.60 [11.95]
Klebsiella_aerogenes_strain_AR_0007_chromosome	74.60 [58.02]	84.48 [12.33]
Klebsiella_aerogenes_strain_AR_0009_chromosome	74.63 [58.39]	84.29 [12.48]
Klebsiella_aerogenes_strain_AR_0018_chromosome	74.64 [57.90]	84.27 [12.39]
Klebsiella_aerogenes_strain_AR_0062_chromosome	74.62 [58.41]	84.46 [12.51]
Klebsiella_aerogenes_strain_AR_0161_chromosome	74.61 [58.17]	84.54 [12.26]
Klebsiella_aerogenes_strain_AUH-KAM-9_chromosome	74.64 [57.86]	84.39 [12.30]
Klebsiella_aerogenes_strain_FDAARGOS_139_chromosome	74.63 [58.38]	84.37 [12.51]
Klebsiella_aerogenes_strain_FDAARGOS_152_chromosome	74.63 [58.37]	84.29 [12.50]
Klebsiella_aerogenes_strain_FDAARGOS_327_chromosome	74.63 [58.38]	84.29 [12.50]
Klebsiella_aerogenes_strain_FDAARGOS_513_chromosome	74.58 [58.38]	84.45 [12.39]
Klebsiella_aerogenes_strain_FDAARGOS_641_chromosome	74.56 [58.37]	84.40 [12.27]
Klebsiella_aerogenes_strain_G7_chromosome	74.62 [58.37]	84.38 [12.50]
Klebsiella_aerogenes_strain_HNHF1_chromosome	74.55 [58.33]	84.42 [12.43]
Leclercia_adecarboxylata_strain_R25	75.20 [60.43]	84.05 [15.04]
Leclercia_sp._4-9–1-25_chromosome	74.98 [58.23]	84.01 [13.94]
Leclercia_sp._29361_chromosome	75.16 [59.88]	84.07 [14.62]
Lelliottia_jeotgali_strain_PFL01	75.46 [61.22]	84.11 [16.55]
Lelliottia_sp._WB101_chromosome	75.46 [61.17]	84.09 [16.1]
Pantoea_rwandensis_strain_ND04	72.46 [44.87]	84.89 [6.39]
Raoultella_planticola_strain_S25_chromosome	74.80 [58.15]	84.50 [12.46]
Raoultella_terrigena_strain_JH01_chromosome	74.63 [57.62]	84.29 [11.55]
Scandinavium_goeteborgense_strain_CCUG_66741_chromosome	75.26 [59.14]	84.21 [15.82]

According to the relevant studies, there are many genera of soil bacteria having the ability to dissolve P, including *Pseudomonas*, *Burkholderia, Bacillus*, *Rhizobium, Enterobacter*, *Agrobacterium*, *Penicillium*, *Aspergillus, Actinomyces*, and *Arbuscules* (Kalayu 2019; Kumar et al. 2014; Mohamed et al. 2019). Different phosphorus-dissolving microorganisms have diverse phosphorus-dissolving mechanisms, and most of them dissolve phosphorus by secreting several substances. In the current study, three phosphate-solubilizing bacteria were isolated from the rhizosphere soil of *T. grandis*. Based on the 16S rRNA sequencing and identification of their phylogenetic relationships, the three PSBs (W1, W74, and W83) were identified as *Pseudomonas*, *Burkholderia*, and *Buttiauxella*, respectively. Comparison of protein sequences against the NR database also indicated that the isolated W1 strain sequence was highly similar to *Pseudomonas sp.,* while W74 showed maximum similarity with *Bacillus subtilis.* Furthermore, W83 was highly similar to *Buttiauxella* (Fig. 4). These results were different from the previous phylogenetic analysis. The possible reason could be that many protein sequences in the NR database have not been verified, and their reliability needs to be improved. Therefore, the final results were deduced based on the phylogenetic analysis. *Pseudomonas* is known as one of the most efficient phosphorus-dissolving bacteria (Rodríguez and Fraga 1999: Kalayu 2019). Previous studies have shown the isolation of different *Pseudomonas* species, such as *Pseudomonas putida* and *Pseudomonas fluorescens,* and proved in laboratory and field experiments that they can promote the root and bud growth of species including rape and tomato, and increase the yield of species, such as potato, rice, apple, citrus, tomato, lettuce, and radish (Rodríguez and Fraga 1999). Bacterial strains of the *Burkholderia* genus were

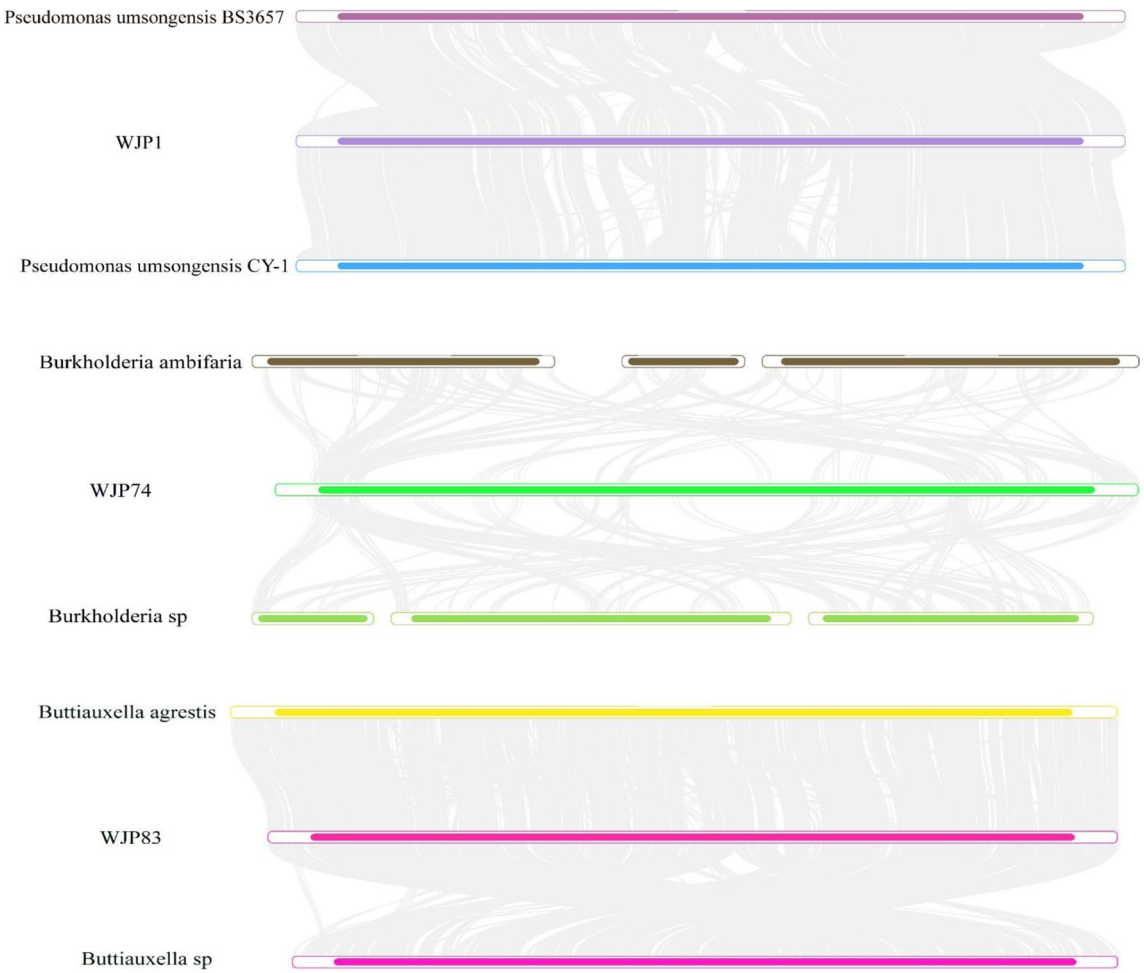

Fig. 7 Global comparison of the whole genome of three strains of bacteria

isolated from different sources at different places and found to have the ability to dissolve inorganic P. For example, two *Burkholderia* species were isolated from high-P iron ore in Brazil (Delvasto et al. 2006). A strain of *Burkholderia* was isolated from the Sichuan corn rhizosphere (Zhao et al. 2014). In addition, two *Burkholderia* strains were isolated from Stevia (Mamta et al. 2010). In some countries, *Burkholderia* is used as a bio-fertilizer in the cultivation of different crops. To the best of our knowledge, this is the first report on P-dissolving microorganisms isolated from *Torreya grandis*, though previous studies have reported the isolation of PSMs from the rhizosphere soil of other plants. For instance, bacteria with P-dissolving ability have been isolated from peanut plants (Anzuay et al. 2013). Five endophytes with different P-dissolving abilities were isolated from cassava roots (Chen et al. 2014). Furthermore, six strains of P-solubilizing bacteria were isolated from the rhizosphere of sweet potato (Ding et al. 2021).

PSB can release organic acids into the soil, thereby reducing soil pH, dissolving mineral phosphate, and promoting plant growth and development (Oteino et al. 2015). In addition, PSB can also help plants to absorb trace elements such as zinc and copper through their roots by secreting organic acids, and thus stimulate their growth and enhance plant resistance to abiotic stresses, such as drought, cold, and salt (Chaiharn and Lumyong 2008). Previous studies have shown that the increase of P concentration in the medium of P-dissolving microorganisms may be related to the secretion of organic acid metabolites (Chouyia et al. 2020; Penn and Camberato 2019). In the current study, measurement of organic acids showed that P-dissolving bacteria secrete a large amount of lactic acid, succinic acid, tartaric acid, etc. in the soil to dissolve insoluble P (Fig. 2). These findings were consistent with the results of existing studies (Rodrıguez a et al. 2000; Jiang et al. 2018; Kalayu 2019; Saeid et al. 2018). Different PSBs have unique phosphorus dissolution

mechanisms because the organic acids or other metabolites produced vary greatly among PSBs (Alori et al. 2017). In the past, many studies have shown that many organic acids participate in the dissolution of phosphorus, but most of them are the intermediate compounds or derivatives of the tricarboxylic acid cycle (Arcand and Schneider 2006; White and Metcalf 2007), such as gluconic acid and citric acid produced by microorganisms, and citric acid, oxalic acid, and malic acid most often produced by plants (Richardson 2001; Ryan et al. 1995; Zheng et al. 2005). In this study, succinic acid was identified as the only product of the tricarboxylic acid cycle. Lactic acid and tartaric acid are neither the tricarboxylic acid cycle compounds nor their derivatives, and the content of lactic acid and tartaric acid was significantly higher than succinic acid. Therefore, we infer that acidification may not be the only mechanism for the phosphorus solubilizing bacteria isolated from the rhizosphere soil of *T. grandis*, and chelation may also play a possible role in P dissolution.

Because the strength of the strain's ability to dissolve phosphorus does not directly represent the strength of its ability to promote plant growth, this study also measured the secretion of IAA for the strain with strong ability to dissolve phosphorus. It was found that three P-dissolving bacteria isolated in this study not only promote the dissolution of insoluble P in the soil but also have additional plant growth-promoting properties, which could be linked to the secretion of IAA (Table 1).

GO analysis showed that biological processes were the main processes in all three strains, and metabolic processes were mainly enriched among the biological processes (Fig. 5). It shows that the three phosphorus-dissolving bacteria strain have strong physiological metabolism and might be in a rapid growth period. In our study, KEGG enrichment analysis showed that ten pathways including carbon metabolism and purine metabolism were significantly enriched (Fig. 6). Altogether, the whole-genome sequencing analysis of the three phosphorus-dissolving bacteria provided data and theoretical support for the subsequent functional genomics research. These findings would promote further research on the phosphorus-dissolution mechanism of PSBs and provide solutions to the problem of phosphorus deficiency in the soil subtropical zone.

In comparative genomic analysis, W1 and *Pseudomonas umsonensis*, W83 and *Buttiauxella agristis* showed a close collinearity relationship, while the colinear relationships of W74 were found to be weaker than the former two. The collinearity analysis of the three strains with other plant species showed that although they were very similar, they could be distinguished, indicating that there were still many diverse genes in the genome. Thus, we suspect that these different genes may be the key factors that cause the ability of phosphorus dissolution between strains and the ability of promoting plant growth, which also needs further verification by subsequent experiments.

Conclusions

We found that the three phosphate-solubilizing bacteria mainly secreted a large number of organic acids to dissolve insoluble phosphorus and increase the soluble phosphorus content that can be absorbed and utilized by plants. In addition, they also secreted a large amount of IAA to promote plant growth and development. GO analysis showed that the metabolic process was the main part of their mechanism, and KEGG analysis showed that carbon metabolism and purine metabolism were highly enriched during the metabolic process. Sequencing the whole genome of the three bacterial strains may open a new direction for solving the problem of phosphorus deficiency in subtropical soils.

Supplementary Information The online version contains supplementary material available at https://doi.org/10.1007/s10123-023-00393-7.

Author contribution JiaSheng Wu and WeiWu Yu: provides Funding acquisition and Project administration. Chenliang Yu, Qi Wang, and WeiWu Yu: did formal analysis. Qi Wang: investigation, data curation. CongCong Kong and Hao Zeng: data curation and visualization. Qi Wang, Chenliang Yu, WeiWu Yu, and JiaSheng Wu: did the manuscript writing and review. All authors contributed to the article and approved the submitted manuscript.

Funding This work was supported by the "Pioneer" and "Leading Goose" R&D Program of Zhejiang(2022C02009 and 2022C02061); the National Natural Science Foundation of China (Grant no. 32171830,); The Breeding of New Varieties of Torreya grandis Program (2021C02066-11); Scientific R&D Foundation for Talent Start-up Project of Zhejiang A&F University (2020FR073).

Data availability The data presented in the study are deposited in the NCBI's SRA repository, BioProject number PRJNA891368 (W1 genome), PRJNA891423 (W74 genome) and PRJNA891438 (W83 genome).

Declarations

Conflict of interest The authors declare no competing interests.

References

Alori ET, Glick BR, Babalola OO (2017) Microbial phosphorus solubilization and its potential for use in sustainable agriculture. Front Microbiol 8:971

Anzuay MS, Frola O, Angelini JG, Ludueña LM, Fabra A, Taurian T (2013) Genetic diversity of phosphate-solubilizing peanut (Arachis hypogaea L.) associated bacteria and mechanisms involved in this ability. Symbiosis 60(3):143–154

Arcand MM, Schneider KD (2006) Plant- and microbial-based mechanisms to improve the agronomic effectiveness of phosphate rock: a review. An Acad Bras Ciênc 78(4):791–807

Bhattacharyya PN, Jha DK (2011) Plant growth-promoting rhizobacteria (PGPR): emergence in agriculture. World J Microbiol Biotechnol 28(4):1327–1350

Chaiharn M, Lumyong S (2008) Phosphate solubilization potential and stress tolerance of rhizobacteria from rice soil in Northern Thailand. World J Microboil Biotechnol 25:305–314

Chen BQ, Cui XY, Zhao X, Zhang YH, Piao HS, Kim JH, Lee BC, Pyo HB, Yun YP (2006) Antioxidative and acute antiinflammatory effects of Torreya grandis. Fitoterapia 77(4):262–267

Chen Y, Fan J-B, Du L, Xu H, Zhang Q-H, He Y-Q (2014) The application of phosphate solubilizing endophyte Pantoea dispersa triggers the microbial community in red acidic soil. Appl Soil Ecol 84:235–244

Chouyia FE, Romano I, Fechtali T, Fagnano M, Fiorentino N, Visconti D, Idbella M, Ventorino V, Pepe O (2020) P-Solubilizing Streptomyces roseocinereus MS1B15 With Multiple Plant Growth-Promoting Traits Enhance Barley Development and Regulate Rhizosphere Microbial Population. Front Plant Sci 11:1137

Chungopast S, Thongjoo C, Islam AKMM, Yeasmin S (2021) Efficiency of phosphate-solubilizing bacteria to address phosphorus fixation in Takhli soil series: a case of sugarcane cultivation, Thailand. Plant Soil 460(1–2):347–357

Delvasto P, Valverde A, Ballester A, Igual J, Munoz J, Gonzalez F, Blazquez M, Garcia C (2006) Characterization of brushite as a re-crystallization product formed during bacterial solubilization of hydroxyapatite in batch cultures. Soil Biol Biochem 38(9):2645–2654

Dessaux EGaY (1995) A critical examination of the specificity of the Salkowski reagent for indolic compounds produced by phytopathogenic bacteria. Appl Environ Microbiol 793–796

Ding Y, Yi Z, Fang Y, He S, Li Y, He K, Zhao H, Jin Y (2021) Multiomics reveal the efficient phosphate-solubilizing mechanism of bacteria on rocky soil. Front Microbiol 12:761972

Dong D, Wang H, Xu F, Xu C, Shao X, Li H (2014) Supercritical carbon dioxide extraction, fatty acid composition, oxidative stability, and antioxidant effect of Torreya grandis seed Oil. J Am Oil Chem Soc 91(5):817–825

Fiori J, Amadesi E, Fanelli F, Tropeano CV, Rugolo M, Gotti R (2018) Cellular and mitochondrial determination of low molecular mass organic acids by LC-MS/MS. J Pharm Biomed Anal 150:33–38

Islam MK (2019) Isolation and molecular characterization of phosphate solubilizing filamentous fungi from subtropical soils in Okinawa. Appl Ecol Environ Res 17(4):9145–9157

Izhar Shafi M, Adnan M, Fahad S, Wahid F, Khan A, Yue Z, Danish S, Zafar-ul-Hye M, Brtnicky M, Datta R (2020) Application of single superphosphate with humic acid improves the growth, yield and phosphorus uptake of wheat (Triticum aestivum L.) in Calcareous Soil. Agronomy 10(9):1224

Jiang H, Qi P, Wang T, Wang M, Chen M, Chen N, Pan L, Chi X (2018) Isolation and characterization of halotolerant phosphate-solubilizing microorganisms from saline soils. 3 Biotech 8:461

Kalayu G (2019) Phosphate solubilizing microorganisms: promising approach as biofertilizers. Int J Agron 2019:1–7

Khan MS, Zaidi A, Ahemad M, Oves M, Wani PA (2010) Plant growth promotion by phosphate solubilizing fungi – current perspective. Arch Agron Soil Sci 56:73–98

Klupczynska A, Plewa S, Sytek N, Sawicki W, Derezinski P, Matysiak J, Kokot ZJ (2018) A study of low-molecular-weight organic acid urinary profiles in prostate cancer by a new liquid chromatography-tandem mass spectrometry method. J Pharm Biomed Anal 159:229–236

Kumar S, Bauddh K, Barman SC, Singh RP (2014) Amendments of microbial biofertilizers and organic substances reduces requirement of urea and DAP with enhanced nutrient availability and productivity of wheat (Triticum aestivum L.). Ecol Eng 71:432–437

Liang JL, Liu J, Jia P, Yang TT, Zeng QW, Zhang SC, Liao B, Shu WS, Li JT (2020) Novel phosphate-solubilizing bacteria enhance soil phosphorus cycling following ecological restoration of land degraded by mining. ISME J 14:1600–1613

Mamta RP, Pathania V, Gulati A, Singh B, Bhanwra RK, Tewari R (2010) Stimulatory effect of phosphate-solubilizing bacteria on plant growth, stevioside and rebaudioside-A contents of Stevia rebaudiana Bertoni. Appl Soil Ecol 46:222–229

Manisalidis I, Stavropoulou E, Stavropoulos A, Bezirtzoglou E (2020) Environmental and health impacts of air pollution: a review. Front Public Health 8:14

Mitter EK, Tosi M, Obregón D, Dunfield KE, Germida JJ (2021) Rethinking crop nutrition in times of modern microbiology: innovative biofertilizer technologies. Front Sustain Food Syst 5:606815

Mohamed AE, Nessim MG, Abou-el-seoud II, Darwish KM, Shamseldin A (2019) Isolation and selection of highly effective phosphate solubilizing bacterial strains to promote wheat growth in Egyptian calcareous soils. Bull Natl Res Cent 43:203

Ni Q, Gao Q, Yu W, Liu X, Xu G, Zhang Y (2015) Supercritical carbon dioxide extraction of oils from two Torreya grandis varieties seeds and their physicochemical and antioxidant properties. LWT - Food Sci Technol 60:1226–1234

Oteino N, Lally RD, Kiwanuka S, Lloyd A, Ryan D, Germaine KJ, Dowling DN (2015) Plant growth promotion induced by phosphate solubilizing endophytic Pseudomonas isolates. Front Microbiol 6:745

Pawlak M, Klupczynska A, Kokot ZJ, Matysiak J (2019) Extending metabolomic studies of Apis mellifera venom: LC-MS-based targeted analysis of organic acids. Toxins (Basel) 12(1):14

Penn C, Camberato J (2019) A critical review on soil chemical processes that control how soil pH affects phosphorus availability to plants. Agriculture 9(6):120

Pradhan A, Pahari A, Mohapatra S, Mishra BB (2017) Phosphate-solubilizing microorganisms in sustainable agriculture: genetic mechanism and application. Adv Soil Microbiol: Recent Trends Future Prospects Microorganisms Sustain 4:81–97

Richardson AE (2001) Prospects for using soil microorganisms to improve the acquisition of phosphorus by plants. Funct Plant Biol 28(9):897

Richardson AE, Simpson RJ (2011) Soil microorganisms mediating phosphorus availability update on microbial phosphorus. Plant Physiol 156:989–996

Rodríguez H, Fraga R, Gonzalez T, Bashan Y (2006) Genetics of phosphate solubilization and its potential applications for improving plant growth-promoting bacteria. Plant Soil 287:15–21

Rodrıguez a H, Gonzalez a T, Sb G (2000) Expression of a mineral phosphate solubilizing gene from Erwinia herbicola in two rhizobacterial strains. J Biotechnol 84(2):155–161

Rodríguez H, Fraga R (1999) Phosphate solubilizing bacteria and their role in plant growth promotion. Biotechnol Adv 17(4–5):319–339

Ryan P, Delhaize E, Randall P (1995) Characterisation of Al-stimulated efflux of malate from the apices of Al-tolerant wheat roots. Planta 196(1):103–110

Saeid A, Prochownik E, Dobrowolska-Iwanek J (2018) Phosphorus solubilization by Bacillus species. Molecules 23(11):2897

Santana EB, Marques EL, Dias JC (2016) Effects of phosphate-solubilizing bacteria, native microorganisms, and rock dust on *Jatropha curcas* L. growth. Genet Mol Res 15(4):gmr.15048729

Sharma SB, Sayyed RZ, Trivedi MH, Gobi TA (2013) Phosphate solubilizing microbes: sustainable approach for managing phosphorus deficiency in agricultural soils. SpringerPlus 2:587

Smith (1999) Host variation for interactions with beneficial plant associated microbes. Ann Rev Phytopathol 37:743–491

Soumare A, Boubekri K, Lyamlouli K, Hafidi M, Ouhdouch Y, Kouisni L (2019) From isolation of phosphate solubilizing microbes to their formulation and use as biofertilizers: status and needs. Front Bioeng Biotechnol 7:425

Tian J, Ge F, Zhang D, Deng S, Liu X (2021) Roles of phosphate solubilizing microorganisms from managing soil phosphorus

deficiency to mediating biogeochemical P cycle. Biology (Basel) 10(2):158
Wang Y, Wang F, Lu H, Liu Y, Mao C (2021) Phosphate uptake and transport in plants: an elaborate regulatory system. Plant Cell Physiol 62:564–572
White AK, Metcalf WW (2007) Microbial metabolism of reduced phosphorus compounds. Ann Rev Microbiol 61(1):379400
Wissuwa M, Gonzalez D, Watts-Williams SJ (2020) The contribution of plant traits and soil microbes to phosphorus uptake from low-phosphorus soil in upland rice varieties. Plant Soil 448:523–537
Xing Y, Shi W, Zhu Y, Wang F, Wu H, Ying Y (2021) Screening and activity assessing of phosphorus availability improving microorganisms associated with bamboo rhizosphere in subtropical China. Environ Microbiol 23:6074–6088
Xu H, Zhang H, Fan Y, Wang R, Cui R, Liu X, Chu S, Jiao Y, Zhang X, Zhang D (2022) The purple acid phosphatase GmPAP17 predominantly enhances phosphorus use efficiency in soybean. Plant Sci 320:111283
Zhao K, Penttinen P, Zhang X, Ao X, Liu M, Yu X, Chen Q (2014) Maize rhizosphere in Sichuan, China, hosts plant growth promoting Burkholderia cepacia with phosphate solubilizing and antifungal abilities. Microbiol Res 169:76–82
Zheng SJ, Yang JL, He YF, Yu XH, Zhang L, You JF, Shen RF, Matsumoto H (2005) Immobilization of aluminum with phosphorus in roots is associated with high aluminum resistance in buckwheat. Plant Physiol 138(1):297–303